Eur. Phys. J. E (2013) **36**: 30
DOI 10.1140/epje/i2013-13030-3

THE EUROPEAN PHYSICAL JOURNAL E

Regular Article

Confined flows of a polymer microgel

Baudouin Geraud, Lyderic Bocquet, and Catherine Barentin[a]

Institut Lumière Matière, UMR5306 Université Lyon 1-CNRS, Université de Lyon 69622 Villeurbanne cedex, France

Received 7 January 2013
Published online: 28 March 2013 –

Abstract. In this paper, we probe the influence of confinement on the flows of a polymer microgel, namely Carbopol. We compare its bulk rheological behavior, measured with a rheometer and well described by a Hershel-Bulkley law, to velocity profiles measured in rough microchannels, obtained with a particle tracking velocimetry technique. We show a strong disagreement between the bulk prediction for the velocity profiles and the measured ones in the microchannels. Velocity profiles in confined conditions are successfully analyzed within the framework of a non-local fluidity model introduced recently (J. Goyon *et al. Nature*, **454**, 84 (2008)). This allows to determine a cooperativity length ξ, whose order of magnitude compares with the structure size of the microgel. Moreover, we measure flow curves using a rheometer for different gap conditions and also show that this set of data exhibit a strong effect of the confinement on the measured rheological properties. This is again characterized by a typical length of the same order as the cooperativity length scale ξ. We thus evidence confinement effects with two complementary experiments which both give the same typical length for the rearrangements in the flows.

1 Introduction

Yield stress fluids (YSF) such as gels, pastes or emulsions are ubiquitous in everyday life and are widely used for industrial applications [1]. These materials are made of a set of jammed particles (typically droplets, colloids or polymer blobs) which present a solid-like or a fluid-like behavior depending on their applied shear stress [2–4]. Indeed, if the stress σ is below a critical value, namely the yield stress σ_Y, the material does not flow ($\dot{\gamma} = 0$). Conversely, if the stress is above σ_Y, the material flows, with a typical flow behavior described by the Herschel-Bulkley law (HB) eq. (1)

$$\sigma = \sigma_Y + K\dot{\gamma}^n \qquad (\text{if } \sigma \geq \sigma_Y), \tag{1}$$

where σ_Y is the yield stress, K the consistency and n the HB exponent. This relation characterizes the non-linear response of these pasty fluids although the microscopic mechanisms at the origin of their flows are still under studies.

In this paper, we are interested in probing the dynamical properties of such complex systems when they are confined, *i.e.*, when the typical length scale of the flow or the channel is on the order of several times the typical microstructure size of the system. On short length scales, cooperative effects such as particle rearrangements may have an influence on the global flow and thus give a tool to study the properties of the YSF. These complex dynamics have been recently observed in various systems such as foams [5–7], colloidal suspensions [8], concentrated emulsions [9–11] or granular materials [12–14]. Some of them could be rationalized on the basis of a non-local fluidity model, which was introduced recently [9,15]. There is accordingly a strong effort in the literature to assess the validity and/or the generality of this non-local description: the final aim is to propose a consistent framework for the flow behaviour of yielding materials, which do not exist up to now and would be essential for application purposes, such as flows in "thin" films of yielding fluids (*e.g.* for coatings with creams or gels).

Polymer microgels, such as Carbopol, are interesting alternative YSF systems. These microgels can be viewed as an assembly of soft polymer blobs [16], and it is accordingly interesting to explore weither, and how, this specific granularity may impact the flow of such systems when confined. Such question has never been addressed in the flow of microgels. Therefore, we study in this paper the influence of the confinement on the flow of a Carbopol microgel, with the aim of probing non-local effects and their description using the fluidity framework. Carbopol is a non-aging and non-thixotropic microgel [17], for which the large-scale rheology is well described by HB law [18–20] and whose structure begins to be well understood [16]. Furthermore, it is a highly elastic and smooth system, which makes it a good candidate to compare its confinement effects with harder systems like colloidal suspensions [8]. Another advantage of Carbopol is

[a] e-mail: catherine.barentin@univ-lyon1.fr

its transparency which allows optical techniques to probe its dynamical properties. Moreover, we can easily play on its microstructure by changing some parameters such as polymer concentration [16]. By this way, we can vary the typical size of the microstructure and thus any confinement effect.

In this article, we evidence confinement effects of Carbopol flows by two different ways and we rationalize our experimental results with the non-local fluidity model [9, 21]. In the first section, we describe the preparation of the samples. In the second part, we present the bulk rheological measurements and we show that confinement effects can be highlighted using rheometer in a Plane Plane (PP) geometry by decreasing the gap between the two planes. This observation leads to consider local measurements of confined flows more in detail, as presented in the third section where a microparticle tracking velocimetry experiment is described. In the fourth section, we point out a strong disagreement between the measured local flows and the ones predicted by the macroscopic rheology. We also show that the confined velocity profiles cannot be described in terms of an *effective* HB law. This leads to consider the non-local model [21] presented in the last part, which rationalizes the experimental results and provides a typical size for the rearrangements in the sheared Carbopol.

2 Microgel preparation

Carbopol powder contains homo- and copolymers of acrylic acid highly cross-linked with a polyalkyl polyether [22,23]. Once the polymer is dispersed into water, adequate *p*H conditions lead to polymer swelling. Swollen polymer particles get jammed into an amorphous assembly referred to as a microgel. Its microstructure can be described as a set of polymer blobs of a few microns in size, and depends among other things on polymer concentration, the chemical base used for neutralization or the stirring rate after preparation [22–24,16]. We chose to vary these three parameters to probe the influence of the gel microstructure on our experiments.

Preparation protocol.– We first disperse carboxylated fluorescent colloids (Fluorescent Microspheres, Molecular Probes) of 1 μm diameter in pure water. The volume fraction of colloids in water is about $\phi = 2 \cdot 10^{-5}$. These colloids play the role of tracers for the local velocimetry detailed in sect. 4. We heat the solution at 50 °C and then dissolve Carbopol ETD 2050 powder with a magnetic stirrer for 30 min. We prepared different samples of 0.25, 0.5 and 1% wt mass fractions. At this stage, the *p*H of the solution is around 3 because of the release of H^+ ions by the acidic functions of the polymer. We let the solution equilibrate at room temperature for 30 min. We neutralize the solution either with sodium hydroxyde (NaOH) or with triethanolamine (TEA), until the *p*H reaches a value of 6.5 ± 0.2. The final *p*H value has low influence on the flow properties of Carbopol ETD 2050 provided it is in the range $5 < p\text{H} < 9$ [16]. The sample is then stirred just by hand for few minutes or by a mixer (RW20, Ika, tip: R1303) at a high stirring rate of 2100 rpm for 24 h. Accordingly, we modify the gel microstructure, the high stirring breaking the larger polymer blobs in smaller ones. All samples are finally centrifuged at 3200 rpm for 10 min to remove air bubbles of the bulk. Table 1 details the parameters that we chose for the preparation of the samples.

Table 1. Summary table of the different parameters used to prepare the samples. The high-stirring procedure induces a homogeneous structure of the microgel contrary to the hand-stirring process.

Sample	Mass fraction	Stirring	Base
A1	0.25%	2100 rpm for 24 h	NaOH
A2	0.5%	2100 rpm for 24 h	NaOH
A3	1%	2100 rpm for 24 h	NaOH
B	0.5%	2100 rpm for 24 h	TEA
C1	0.5%	hand-stirred	NaOH
C2	0.5%	hand-stirred	TEA

3 Macroscopic rheology

In this part, we study the bulk rheology of the samples with a rheometer in a PP geometry instead of the usual Cone-Plane (CP) geometry for which the stress and the shear rate are homogeneous. We chose this configuration because PP geometry allows us to study the influence of the confinement on the macroscopic rheological properties by just changing the gap between the two planes. Moreover, its is easier to control the roughness of the planes and so to control the slip of the complex fluids. However commercial rheometers are designed for measurements on Newtonian fluids, which can lead to errors in the flow curves of non-Newtonian material due to the stress inhomogeneity in PP geometry. A correction of this effect is necessary to get the *actual* HB coefficient values, as suggested and verified by different authors [25–27]. This correction is particularly important in our case, since we compare the macroscopic flow properties of a non-Newtonian fluid with its flow in microchannels as shown in sect. 4. This correction is detailed and verified on Carbopol samples in appendix A. In the following, we present the rheological measurements, as well as the procedure that we used to prepare our samples, and we show that confinement effects are also observed using a rheometer.

3.1 Rheological measurements

The macroscopic flow curves were obtained with a stress-controlled rheometer (MCR301, Anton Paar) set up with a PP geometry. The planes are 21.5 mm disks on which a 46 μm roughness sandpaper has been glued to avoid slippage as mentioned before. The sample is successively presheared at $500\,\text{s}^{-1}$ and $-500\,\text{s}^{-1}$ for 1 min at each step

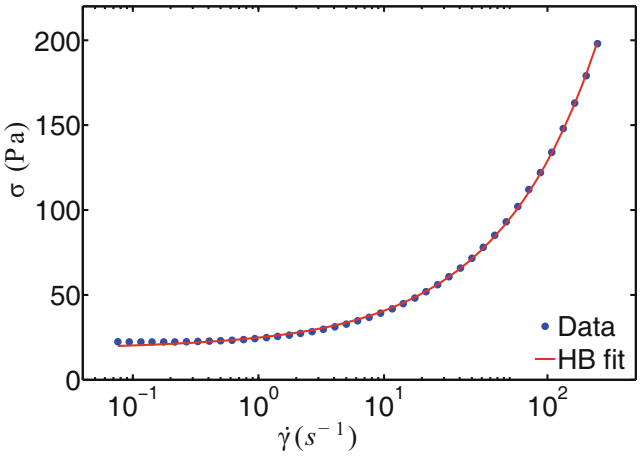

Fig. 1. Macroscopic flow curve of Carbopol 1% wt, swelled with NaOH and stirred for 24 h at 2100 rpm, before correction due to the stress inhomogeneity: the points correspond to the experimental data obtained with rough PP (46 μm). The plain curve corresponds to the HB fit. Each point of the flow curve is measured over 100 s.

Table 2. HB coefficients of all the studied samples measured with a PP 46 μm roughness rheometer, with 1 mm gap and after correction.

Sample	σ_Y (Pa)	n	K (SI)
A1	1.15	0.558	1.39
A2	4.22	0.558	2.54
A3	13.73	0.534	5.79
B	3.89	0.521	3.35
C1	12.10	0.507	8.10
C2	11.82	0.498	8.19

and then let at rest for 2 min 30 s to let the system relax. This is the same protocole as used in previous studies on Carbopol [28,20]. The flow curves are measured at fixed shear rates ranging usually from 0,05 s^{-1} to 500 s^{-1} starting from the high shear rates. Each point of the flow curve is measured over 100 s. We first fixed the gap between the two planes to 1 mm.

As shown in fig. 1, the flow curve of Carbopol is well fitted by an Herschel-Bulkley law and table 2 gathers the values of the HB coefficients after correcting the stress inhomogeneity for all samples that we used.

The fitting HB parameters vary with the sample preparation, showing that the polymer microstructure changes as well. The values obtained with samples A1, A2 and A3 show that for a same stirring rate and a same base, increasing the polymer concentration results in an increase of the yield stress and of the consistency as already observed [22,29,16,30]. The comparison between samples A2 and C1 or B and C2 shows that a high stirring during the preparation results in lower yield stress and lower consistency, meaning that the samples become more fluid-like when they are hardly stirred [23]. Finally, the comparison

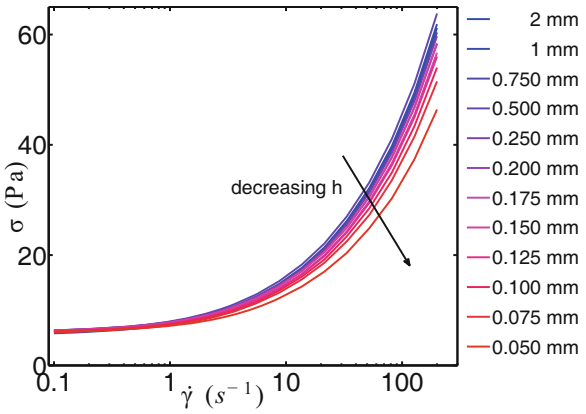

Fig. 2. Influence of the gap values on the flow curves of Carbopol 0.5% wt, swelled with NaOH and stirred for 24 h at 2100 rpm in rough PP geometry (20 μm). Each point is obtained over 30 s.

between samples A2 and B or C1 and C2 shows that the nature of the chemical base used to swell the polymers has *a priori* low influence on their bulk properties.

3.2 Signature of the confinement on the rheological parameters

In this part, we want to check whether any confinement effect can be observed with a rheometer. To answer this question, we performed rheological measurements on a sample of 0.5% wt Carbopol, stirred at 2100 rpm for 24 h. This sample is similar to the A2 one except that it has no colloid seeded inside. For these experiments, we used 20 μm rough disks instead of the 46 μm ones to have a lower roughness/gap ratio when the gap is small. Figure 2 gathers the rheological curves obtained with 12 different gap values, ranging from 2 mm (typical bulk orders of magnitude) to 50 μm where the fluid is confined. The flow curves are measured according to the same procedure described in the previous part excepted that here, each point of the flow curve is measured over 30 s to avoid any drying of the few amount of material when it is confined. For each experiment —that is for each gap value— we controlled the amount of Carbopol set into the two plates with a syringe, to reduce as much as possible the influence of the material ring out of the disks. Our uncertainty on the size of the ring is of half a millimeter and is reported in the corresponding uncertainties of the measures of the consistency and the yield stress.

As shown in fig. 2, the flow curves obtained with gaps of 1 mm and 2 mm coincide, which means that the millimeter is the typical bulk length scale: the fluid is well described by its bulk rheology. This is in good agreement with the work of Divoux *et al.* [20], which noted that Carbopol followed a unique HB law in a 3 mm gap Couette rheometer. However, the rheological curves corresponding to gap values below 500 μm do not collapse on the bulk curve showing a confinement effect. Fitting the flow curves with Herschel-Bulkley laws allows to follow the trend of

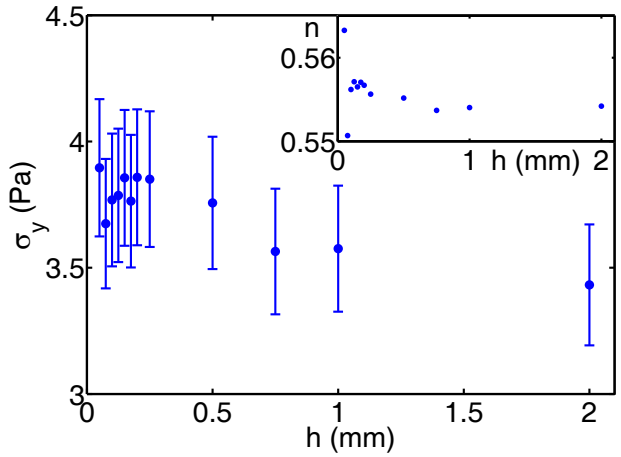

Fig. 3. Evolution of the yield stress and the exponent n, of Carbopol 0.5% wt, swelled with NaOH and stirred for 24 h at 2100 rpm, as a function of the gap between the two planes.

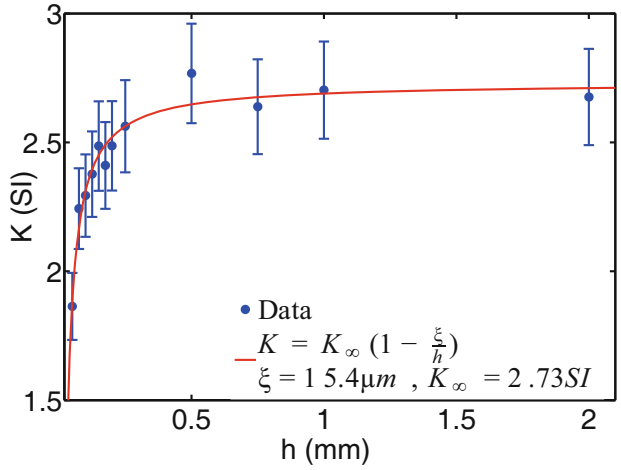

Fig. 4. Evolution of the consistency K, of Carbopol 0.5% wt swelled with NaOH and stirred for 24 h at 2100 rpm, as a function of the gap between the two planes. K presents a strong decrease as the confinement increases. The plain curve corresponds to an algebric fit of the data, allowing to extract a typical length scale of about 15 μm and the bulk consistency.

the parameters with the gap (fig. 3 and 4), although the experimental uncertainties on the coefficients are quite important. Yield stresses and HB exponents exhibit no significant dependence with gap values as shown in fig. 3. There is a slight increase of the yield stress with the confinement but this trend cannot be detected on the flow curves (fig. 2). Note that a strong increase of the yield stress with confinement has already been observed with other yield stress fluids than Carbopol [27]. However, the consistency seems to be a more relevant quantity to evidence the effects of confinement.

Indeed, as shown in fig. 4, measurements show a clear decrease of the consistency as the gap is decreased, which is in good agreement with the data obtained by Yan *et al.* [27]. The evolution of the consistency with the gap values allows a scaling analysis. Data are well described by the the two-parameters fit $K = K_\infty(1 - \frac{\xi}{h})$, with $K_\infty = 2.73 \pm 0.06$ SI which correspond to the bulk value and $\xi = 15.4 \pm 2.2\,\mu$m. This last measure provides a typical length scale characterizing the variations of the flow curves with confinement. Note that, while this length scale ξ is small in comparison with the typical "bulk" length scale (1 mm), confinement effects are still visible for gap values of 250 μm.

Despite the experimental uncertainties, these measurements allow to determine two typical lengths: the gap under which the fluid is confined and a length scale ξ inherent to the fluid which is evidenced by the confinement and which emerges from the scaling analysis. Note that we just present in this section the results concerning a high-stirred sample, whereas the study on a hand-stirred sample is presented in appendix B.

Since the bulk rheological law does not hold for low gaps, it raises the question of the description of the flow under confinement. In particular, we can wonder whether another description of the flows is possible. This question leads to the measurements of the local flow which is presented in the next section, including the description of the experimental set up and of the data processing used to obtain the velocity profiles and the local rheology of such fluids.

4 Velocity Profiles Measurements and local rheology

4.1 Local rheology in a 2D channel

In this section, we use an alternative device with the aim to probe the local properties of confined fluids. We use for this a 2D channel which allows us to know exactly the stress field across the channel once a pressure difference is set along it. Indeed, if the aspect ratio width/height of the channel is small enough, the channel can be considered as a 2D system so that the shear stress is fixed by mechanical equilibrium and follows

$$\sigma(x) = \nabla P \cdot x, \qquad \text{with} \qquad \nabla P = \frac{\Delta P}{L}, \qquad (2)$$

where ∇P is the pressure difference along the channel, L the channel length and x is the position between the two walls as defined in fig. 5. This relation implies that once the pressure difference is fixed, the stress is known at every point across the channel. Moreover, measuring the velocity profile $v(x)$, we can access to the shear rate $\dot{\gamma}(x) = \frac{\mathrm{d}v}{\mathrm{d}x}(x)$ and then to the local rheology $\sigma(\dot{\gamma}(x))$. This procedure allows to compare the microscopic rheology of the fluid to its macroscopic one measured with the rheometer [9]. The velocity profiles are obtained by following the displacements of the fluorescent colloids seeded in the samples. The movies of the flows are recorded with the aid of a PIV-experiment set-up which is detailed in the next part.

Flows of Carbopols are known to present large slip on smooth surfaces without any specific treatment [31] and the fluid is not sheared enough to conclude anything on

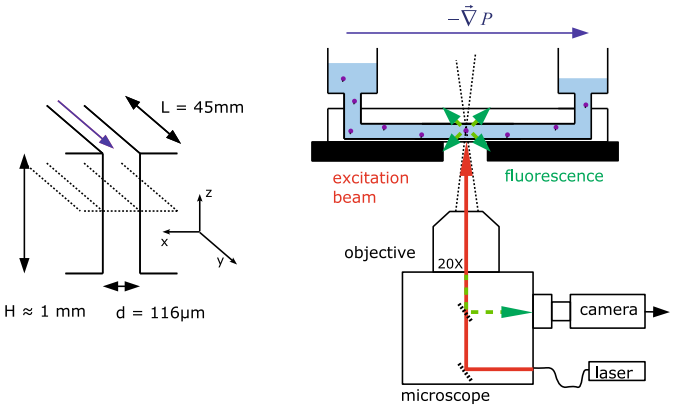

Fig. 5. Scheme representing the channel dimensions and the experimental set-up. The channel presents a high aspect ratio so that the flow can be considered as 2D.

its microscopic rheology. So, we drove the flows in rough microchannels so we could measure a sufficient shear rate across the channel section $\dot{\gamma}(x)$. Accordingly the ratio slip velocity/maximum velocity is at worst of 15% while it is of order of 90% for Carbopol flows in glass capillaries for which we have almost pure plug flows.

Channel preparation.– We used rectangular rough glass channels made as described in [32]. Two glass slides of 1 mm thick are separated with a spacer and sealed with another slide with an optical adhesive (NOA81, Norland Products), and a cover slide seals the two glass slides on the other side to allow microscopic observation. Channel dimensions are 1 mm × 116 μm × 45 mm (see fig. 5) and they present a large aspect ratio so that the flow can be described as a 2D flow at the half of its height (*i.e.*, at 500 μm). This implies that eq. (2) applies. Carbopol flows between the two glass slides and slippage is reduced due to the roughness of the glass slices, which has been estimated with AFM measurements: it appears to be made of some spots of some half-microns height separated by about 5 μm.

4.2 Experimental set-up and procedure

The experimental set-up is described in fig. 5. It is composed of a microscope with a 20× objective (NA = 0.4, WD = 6.9 mm), which is set on a piezo-transducer (Märzhäuzer). This piezo controls the position of the observation plane along the z-axis with a precision of 0.1 μm. The position of the focal plane is fixed at 500 μm in the channel, which, given the refractive index of water, corresponds to a translation of 375 μm of the objective. A laser beam (532 nm, 400 mW) is guided and focalized through the microscope on the observation plane in the channel to excite fluorescence of the latex beams during the flow. An Acousto-optic modulator (MT80, R&D vision) shuts the laser while a 8 bit, 640 × 480 pixels camera (Allied Technologies) records the signal. A synchronizer (EG, R&D vision) controls the acquisition frequency f of frame pairs separated by a time interval ΔT. The synchronizer also allows to control the width time duration τ_{pw} of laser pulses and so the brightness of the fluorescent colloids. τ_{pw} is chosen such that their grey level reaches a value of about 150 on images. The volume fraction of colloids seeded in the sample during the preparation corresponds to an average of some tens of colloids per picture during the flow. The size of the lighted zone on pictures is about 80 μm and does not cover the whole channel width, which is estimated by taking a picture at the lower plane. Pictures are directly recorded on a computer disk. The combination of the acousto-optic modulator and the acquisition of frame pairs allowed us to probe a wide range of velocities (up to 6 cm s^{-1} for the A1 sample) and so a wide range of shear rates.

The flow is driven at a fixed pressure difference with a compressor controlled by a generator. A derivation connected with a voltmeter allows to measure accurately the output pressure through a calibration. For once the pressure is ordered with the generator, we wait the output pressure to reach the steady-state regime to begin the measurements. We record about 10^4 frames per fixed pressure difference measurement.

4.3 Data processing

Movies are processed with a particle tracking algorithm (inspired by the one developed by David Grier, John Crocker, and Eric Weeks and adapted to Matlab by Daniel Blair and Eric Dufresne) which allows to get a set of N points of the velocity profile $\{v_{y_i}(x_i)\}_{i=1...N}$. Each velocity profile is usually made of $2 \cdot 10^4$ points. The main steps of the processing are the following: We first apply a threshold on pictures and a 2D filter to reduce noise. Then, the program locates the positions of all the local maxima on the pictures which are supposed to be the colloids. Nonetheless, in a few cases, some optical aberrations (some rings) can also be interpreted as particles at this step. The position of the colloids are computed to sub-pixel resolution with the weighted averages x and y locations of brightened pixels around the local maxima. Finally, the displacements between two pictures are obtained by minimizing the *global* displacement of colloids between two pictures. Because of the dispersion of data, the points are gathered on a set of 30 positions separated by two microns across the channel, giving the final averaged velocity profile $v_y(x)$ as a function of the position in the channel x (fig. 6). The number of points used during this binning process decreases from the wall position to the center of the channels but is of the order of magnitude of 800 for each averaged velocity (fig. 7).

Wall position.– This point is particularly important to determine correctly the wall slip velocity. In our device, the laser spot covers just a bit more than half of the channel, wall included. Because of the wall, some reflections due to clusters of colloids or some optical aberrations can be detected as particles by the program out of the channel as shown in fig. 7. We fix the position of the wall to the

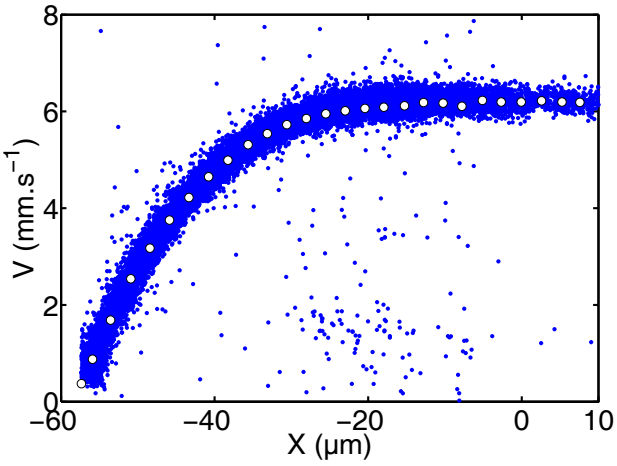

Fig. 6. Result of the binning process on a flow of a Carbopol 1% wt highly stirred (A3) with a pressure drop of 0.88 bar. The blue points are the data obtained after applying the particle tracking process on movies and are about $2 \cdot 10^4$ here. The white points are the averaged values obtained after the binning process.

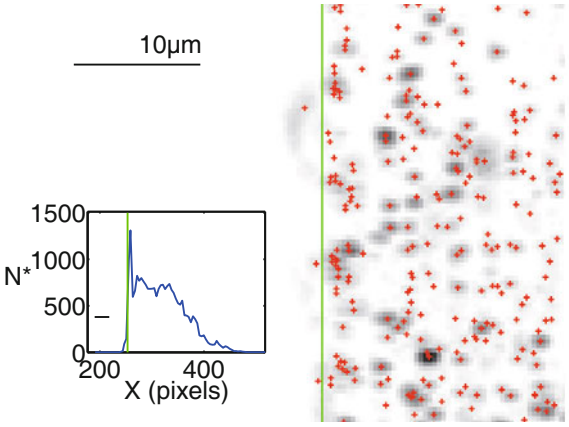

Fig. 7. Right: details of the recorded positions of colloids close to the wall position. The background picture is obtained by keeping the more lighted pixels over 436 frames and then inverting the grey levels. The red crosses are the recorded positions of the colloids after data processing. The green line corresponds to the measured wall position. Note that some optical aberrations have been interpreted as particles out of the channel. Left: number of colloids recorded across the channels N^* for 10^4 pictures. The decrease of N^* across the channel is only due to the Gaussian decrease of the laser intensity, the colloids being less illuminated in the center of the channel.

place where the number of colloids increases dramatically typically above 150 colloids on the corresponding pixel-abscisse over the whole film. Comparison with the movies shows a good agreement between the position of the wall and the computed position, as seen in fig. 7.

Slip velocity.– Slip velocity is obtained by the linear extrapolation of the velocity profiles to the wall. The main source of noise comes from the spreading of the velocity distribution due to the optical aberrations and reflections

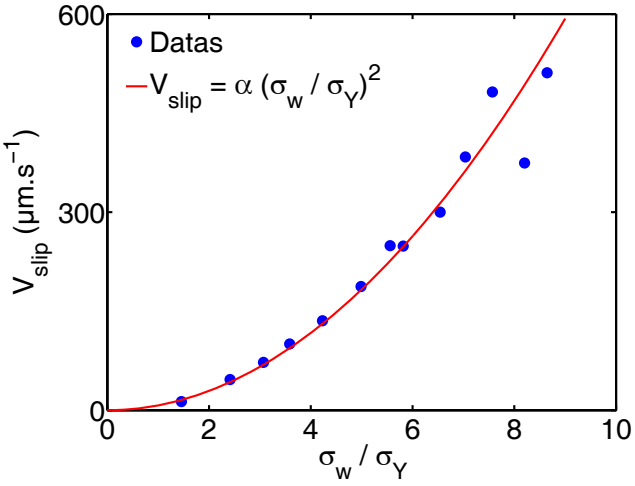

Fig. 8. Solid dots are slip velocities of Carbopol 1% wt (A3) as a function of the ratio between the applied wall shear stress and the macroscopic yield stress. The plain curve is a square fit of the experimental data.

at the wall. The relative error on the slip velocity is directly linked to the error on the value of the shear rates. Indeed, we consider the linear extension of the velocity profile on the wall position, that means that we assimilate the first measured shear rate in the channel $\dot{\gamma}_1$ with the shear rate at the wall $\dot{\gamma}_w$. For an HB fluid characterized by an exponent $1/n \simeq 2$, the relative error on the shear rate is given by

$$\frac{\Delta\dot{\gamma}}{\dot{\gamma}} \approx 2\frac{\Delta\sigma}{\sigma} \approx 2\frac{\Delta x}{x}\,,$$

since $\sigma = \frac{\Delta P}{L}x$. Knowing that $\dot{\gamma}_1$ is estimated at a distance $\Delta x = 1\,\mu$m from the wall and that the location of the wall is at $w = x_w = -58\,\mu$m, the relative errors on the shear rate and on the slip velocity are about 3%.

Figure 8 gathers the slip velocities obtained with the Carbopol 1% wt (sample A3) for several wall shear stresses. We note a good agreement of the measured data with a square law, similar to what predicted by Meeker *et al.* [33,34] for polymer gels, although the walls are rough in our experimental conditions.

5 Experimental results

5.1 Velocity profiles

The velocity profiles are obtained with a pressure difference ranging from 0.15 bar to 1 bar, corresponding to a wall shear stress ranging from 19 Pa and 121 Pa. The maximum velocity recorded in the center of the channel was up to 6 cm s^{-1}. Figure 9 shows the recorded velocity profiles with Carbopol 1% wt (sample A3) for different pressure gradients. The velocity profiles are non-homogeneous: the shear is mostly localized close to the walls and the microgel is barely sheared in the center of the channel. Note that the slippage ratio $V_{\rm slip}/V_{\rm max}$ is quite low, about 10%

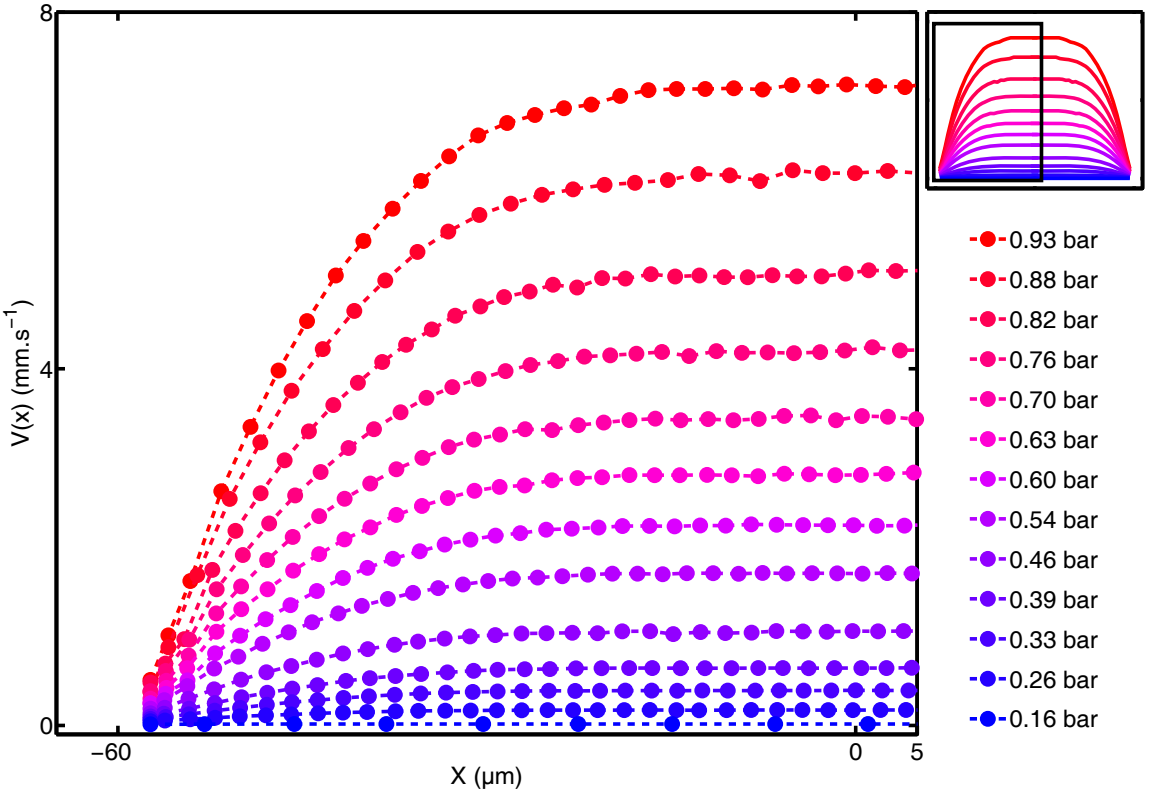

Fig. 9. Set of measured velocity profiles with a Carbopol 1% wt highly stirred (A3), obtained at several pressure differences. The dashed curves are just guides for the eyes.

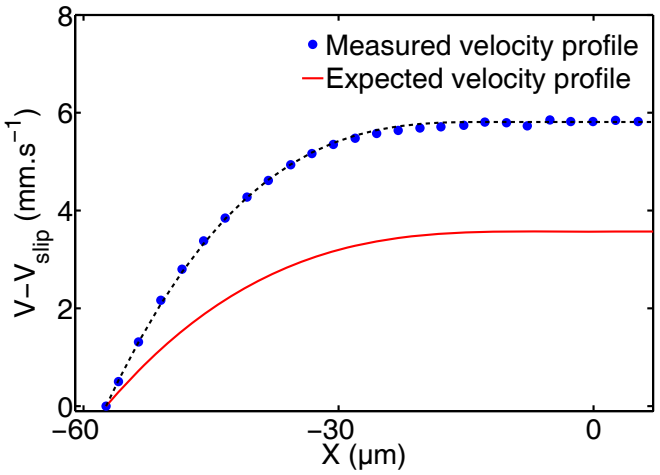

Fig. 10. Solid dots: measured velocity profile for Carbopol 1% wt highly stirred (A3) at $\Delta P = 0.88$ bar. Red line: velocity profile expected from the bulk rheology (HB parameters: $n = 0.53\, K = 5.79$ SI $\sigma_Y = 13.7$ Pa at $\Delta P = 0.88$ bar). Black dashed line: *effective* HB fit with following parameters: $n = 0.53\, K = 3.9$ SI and $\sigma_Y = 22$ Pa.

for most of the flows, which is an effect of wall roughness. Knowing the slip velocity, we can subtract it from the velocity profiles and now compare it to the expected velocity profiles by the macroscopic HB law.

5.2 Comparison with expected velocity profiles: HB fails

In fig. 10, we present a comparison between one velocity profile measured at one pressure with the one calculated using the bulk rheology. The main feature that we observe is an enhancement of the confined flow compared to the velocity profile expected from the bulk measurement. Similar effects have been also observed with concentrated emulsions [9,10]. This demonstrates that *microgel flows cannot be described by their macroscopic flow curve when they are confined*. This flow enhancement is of the order of magnitude of 60% and can reach a value of 70% for the maximum velocity as shown in fig. 11. The relative uncertainty of the velocity ratio is at worst of 10%, well below the flow enhancement.

Fitting the profiles with an effective HB.– Considering that the fluid is barely sheared in the center of the channel, one can wonder whether the observed flow could be described by an HB flow curve, whose parameters would be different from the macroscopic ones. These parameters would be obtained by fitting the velocity profiles with a plug flow equation, obtained by the integrating the HB law

$$v_y(x) = v_{\max}\left\{1 - \sqcap_Y \left(\frac{|x| - |x_Y|}{w - |x_Y|}\right)^{\frac{1}{n}+1}\right\}, \qquad (3)$$

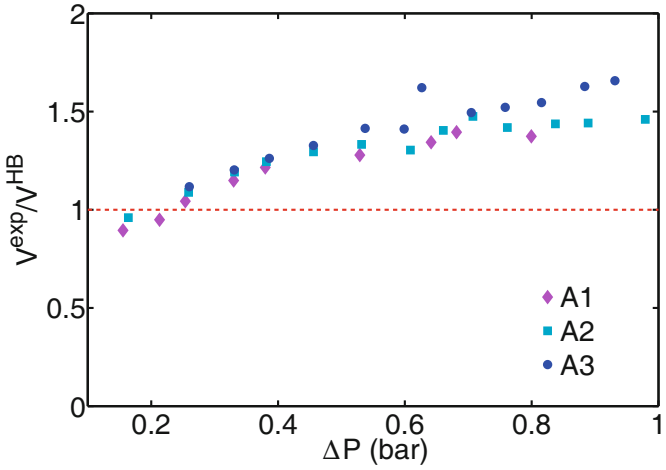

Fig. 11. Evolution of the ratio between the measured maximal velocity and the expected maximum velocity as a function of the pressure difference. Confinement results in a flow enhancement for highly stirred Carbopol of 0.25, 0.5 and 1% wt (respectively A1, A2, A3 samples). The confinement effect slightly increases with concentration and so with the typical structure size [16].

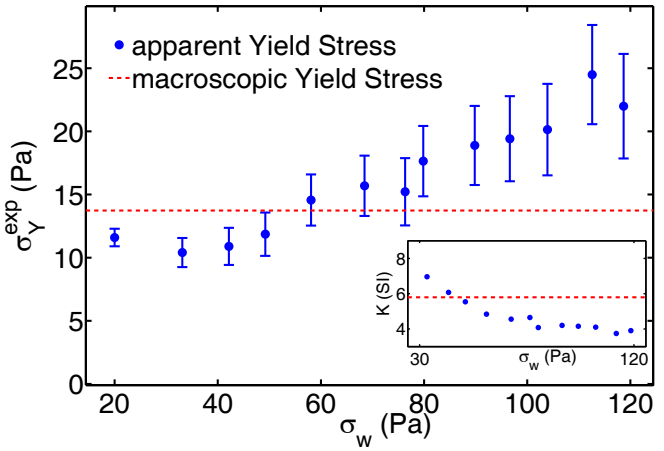

Fig. 12. Evolution of the *effective* yield stress obtained by fitting the velocity profiles with a fixed exponent $n = n_{\text{bulk}}$ as a function of the wall stress. The error bars correspond to $\Delta\sigma = (\nabla P)\cdot\Delta x$, where Δx is the distance separating the points of the velocity profile across the channel. Inset: evolution of the *effective* consistency with the wall stress. The red dashed lines correspond to the macroscopic values measured by the rheometer in high gap conditions.

with a maximum velocity defined by

$$v_{\max} = \frac{n}{n+1}\left(\frac{\nabla P}{K}\right)^{\frac{1}{n}}(w - x_Y)^{\frac{1}{n}+1}. \qquad (4)$$

In those equations, x_Y corresponds to the position where $\sigma(x_Y) = -\sigma_Y$ and $\sqcap_Y$ is a function whose value is 0 if $|x| < x_Y$ and 1 elsewhere. The three parameters of HB (σ_Y, n and K) are hidden in the values of $x_Y = \frac{\sigma_Y}{\nabla P}$ and $v_{\max}$. Fitting the velocity profiles with a three-free-parameters fit is possible but shows that the n exponent changes only a little. Given the experimental uncertainties, we decided to fix the n exponent to the value measured with the bulk rheology. A fit is presented in fig. 10 (black dashed line). For all the samples except the sample B, the effective yield stress measured on the velocity profiles increases with the pressure gradient, whereas the consistency follows the opposite trend as shown in fig. 12. The decrease of the consistency with the pressure indicates that the system is sheared more and more easily as the pressure increases. Note that such a process is artificial since the fitting parameters (σ_Y and K) depend on the value of the pressure difference along the channel. This analysis shows that the confined rheology cannot be described with a single effective HB equation.

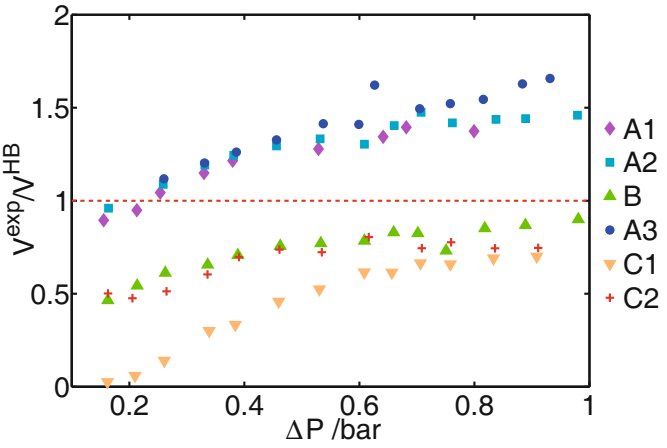

Fig. 13. Ratios between the measured maximal velocity and the expected maximum velocity as a function of the pressure difference for all studied samples. Note that the hand-stirred samples (C1, C2) do not exhibit flow enhancement contrary to the highly stirred Carbopols (A1-A3). This difference of behavior is explained in detail in appendix B.

5.3 Influence of the preparation

We probed the influence of the Carbopol preparation on the observed features with the same protocol as described in sect. 4, and the results are shown in fig. 13. It appears first that highly stirred Carbopols all present flow enhancements, whatever the polymer concentration (respectively 0.25, 0.5 and 1% wt). We mentioned that we prepared samples swelled with two kinds of base (NaOH or TEA) to probe different microstructures. The two kinds of samples seem to have different microscopic behaviors under confinement, despite their bulk properties are quite the same (see table 2 for instance). On the opposite, hand-stirred Carbopols all flow slower than predicted with bulk rheology. This is probably due to the presence of huge clusters of Carbopol which have not been broken during the preparation; such clusters may span the channel over its width and an increased wall friction would thus reduce the flow. This flow reduction was also noted with a rheometer in a confined PP rough geometry as shown in appendix B.

For most of the samples, we note that the velocity ratio $v_{\max}^{\exp}/v_{\max}^{\text{th}}$ increases with the wall shear stress (or the pressure gradient); this is certainly due to an increase of the rearrangements rate with the pressure drop which enhance the confinement effects. Note also that the confinement effects seem to be increased with the concentration. Indeed, by increasing the polymer concentration, one expects to increase the mean size of the polymer blobs [16] and by thus the confinement effect, which is slightly observed between the samples A1, A2 and A3.

To conclude on this part, the measurements show that, in most of the cases, confinement results in flow enhancements which are in full agreement with the measurements performed in PP geometry (fig. 4). These measurements show indeed a decrease of the Carbopol consistency with the confinement which is at the origin of the flow increase. The obtained velocity profile can be fit by a plug flow with an *effective* HB law; but this approach does not make sense since the fit parameters change with the pressure drop driving flow across the channel. Such analysis does not exhibit any typical length scale which allows to rationalize the confinement effect. Another approach to describe confinement effects is to consider a non-local fluidity model [21], as described in the following section.

6 Analysis according the non-local fluidity model

As explained, flows of confined polymer gels can not be described by their bulk rheological properties. We have also seen that interpreting the results with an *effective* rheological law is meaningless since it is impossible to find a single set of parameters describing the flow. Such effects have also been observed with flows of emulsions [9] in a confined geometry and have been interpreted with a non-local model [21]. To assess the validity of this non-local framework, we test this model and use it to analyse our data.

6.1 Non-local fluidity model

This model introduces the key concept of fluidity [21], standing for the inverse of a viscosity, and which is related to the rate of rearrangements in the material during the flow

$$\dot{\gamma} = f\sigma. \tag{5}$$

This constitutive equation is coupled with a stationary equation, representing the diffusion of the rearrangements across the flow

$$\xi^2 \triangle f + f_b[\sigma] - f = 0, \tag{6}$$

where ξ is the cooperativity length, which corresponds to the spatial range of a rearrangement, f is the local fluidity and $f_b[\sigma(x)]$ is the bulk fluidity across the channel, given by the HB macroscopic coefficients

$$f_b[\sigma(x)] = \frac{1}{\sigma(x)}\left(\frac{\sigma(x)-\sigma_Y}{K}\right)^n, \quad \text{if} \quad \sigma(x) > \sigma_Y$$

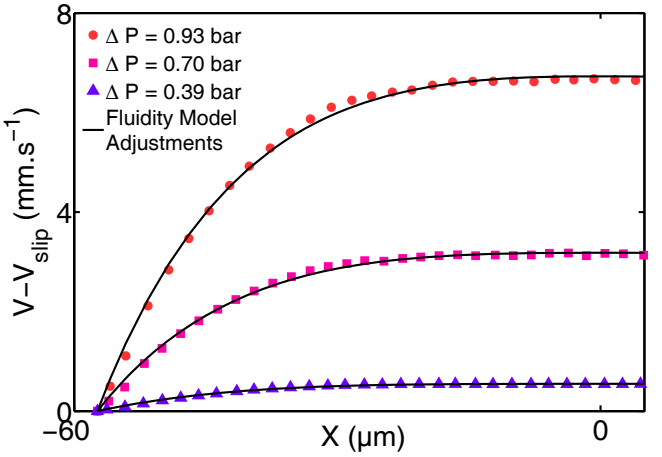

Fig. 14. Fits with eq. (8) of the experimental velocity profiles obtained with Carbopol 1% wt (A3) at several pressure differences: 0.93, 0.7 and 0.39 bar. The corresponding values found for ξ are, respectively, 13.8,12.2 and 11.5 μm

and $f_b[\sigma(x)] = 0$ otherwise.

The physical idea beneath this model is that, contrary to the macroscopic case where spatial variations of the flow are supposed to be large compared to the range of the rearrangements, confined geometries are characterized by rearrangements which can diffuse in the central part of the channel, where the shear stress is below the yield stress. Flows in confined geometry are thus described by a non-local rheology.

Equation (6) is completed with following boundary conditions $f(\pm w) = f_w$ and is implemented by $\partial_x f(x = 0) = 0$ due to symmetry of the problem. Equation and boundary conditions can be solved as

$$f(x) = \frac{\cosh(\frac{x}{\xi})}{\cosh(\frac{w}{\xi})}\left[f_w - \int_0^w f_b[\sigma(x')]\sinh\left(\frac{x'-w}{\xi}\right)\frac{\mathrm{d}x'}{\xi}\right] + \int_0^x f_b[\sigma(x')]\sinh\left(\frac{x'-x}{\xi}\right)\frac{\mathrm{d}x'}{\xi}. \tag{7}$$

Given the pressure gradient (so the shear stress field $\sigma(x) = \nabla P \cdot x$) and the macroscopic rheology of the sample f_b, this equation just depends on ξ and f_w. Among these two parameters, ξ is intrinsic to the material, typically some structure sizes [9,10] and f_w is related to the slope of the velocity profile at the wall. Integrating eqs. (5) and (7) leads to the velocity profile, which depends only on ξ and f_w

$$v(x,\xi,f_w) = \int_{-w}^{x} f(\sigma(x'),\xi,f_w)\cdot\sigma(x')\mathrm{d}x'. \tag{8}$$

6.2 Comparison between measured and calculated velocity profiles

Figure 14 shows three examples of velocity profiles fitted with eq. (8). We apply the same analysis for all velocity

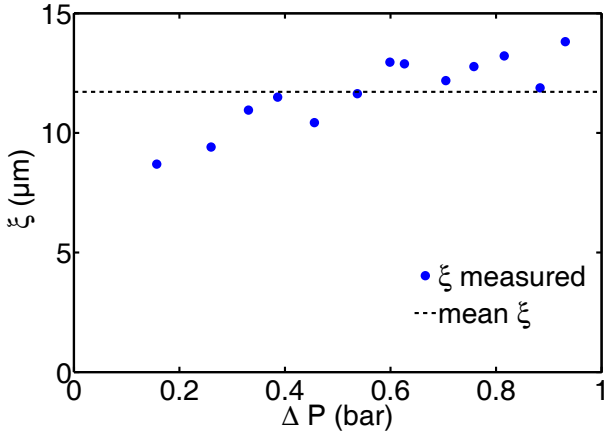

Fig. 15. Influence of the pressure difference on the value of ξ found for Carbopol 1% wt, highly stirred and swelled with NaOH (A3). These values are weakly dispersed around the mean value 11.7 μm.

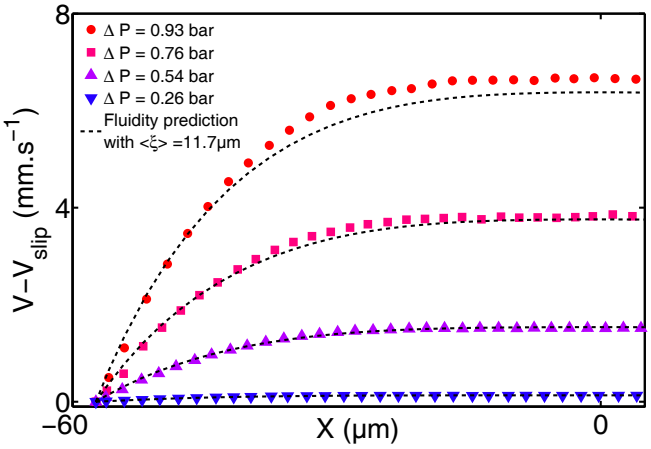

Fig. 16. Comparison between the measured velocity profiles and the ones calculated using the eq. (8) with values f_w found in previous fits (fig. 15) and with an unique cooperativity length ($\xi = 11.7\,\mu$m). The relative error on the maximum velocity is at worst 4%.

profiles and calculated ξ and f_w for all samples and for all pressure differences. It is important to stress the fact that the velocity profiles obtained by (8) are quite sensitive to the value of f_w so that we rather use f_w as a fit parameter instead of measuring it from the slope of the velocity profile at the wall.

For all profiles exhibiting a flow enhancement, the model fits very well the data. The fitting process also allows to measure values of ξ for all the imposed pressure gradients, as shown in fig. 15. These measured values weakly depend on the pressure difference with an average of 11.7 μm. ξ stands for the spatial range of the rearrangements and is in good agreement with some typical structure sizes measured by Lee *et al.* [16]. While there is a slight dispersion in the extracted values of ξ in fig. 14, this has far less impact than the previously extracted dispersion of *effective* HB parameters discussed in the previous section. This is evidenced by plotting the velocity profiles given by the non-local fluidity model with the values of f_w found with the previous fits and by fixing, for *all* profiles, the same cooperativity length ξ to its average value $\langle\xi\rangle = 11.7\,\mu$m. The result is presented in fig. 16 and shows that the profiles are well described and the relative error on the maximum velocity is at worst of 4%. This demonstrates that this non-local model rationalizes well the confinement effect, although more subtle effects such as the slight increase of ξ is not described.

Table 3. Mean values of ξ given by the fits of the velocity profiles with the simple fluidity model.

Sample	ξ (μm)
A1	7.3
A2	13.4
A3	11.7
B	13.16

Table 3 gathers the mean values of ξ found with the fluidity model for the studied samples. Indeed, we managed to fit the velocity profiles of all the samples except the ones which were hand-stirred (C1 and C2). Despite their different behavior in a confined geometry (cf. fig. 13), samples A2 and B present very closed values of ξ. Comparing the values obtained for sample A1 to the others seems to confirm that concentration has an effect on the cooperativity length, which increases with the size of the polymer blobs. The same effect is less obvious between samples A3 and A2/B.

Another important result is that this analysis in terms of non-local rheology gives a cooperativity length value of the same order of magnitude as the one found in the confined PP geometry for a Carbopol sample of the *same concentration* (sect. 3). This demonstrates that the model provides a consistent microscopic interpretation of what happens when the fluid is confined and gives sense to the typical length scale that we exhibited with the rheometer.

7 Conclusion and outlooks

We have shown that confined flows of Carbopol in rough channels exhibit finite-size effects and non-local rheology. Indeed Herschel-Bulckley law —which would be used classically to account for the flow— fails to describe the velocity profiles under confinement. These non-local effects are well described by the fluidity model which allows to extract a typical range of the rearrangements in the sheared Carbopol. Moreover, this typical length ξ was measured independently in a microrheology experiment and in a rheological one, and appears to be intrinsic to the fluid. Nonetheless, there remain many open questions especially on the influence of the structure on this effect. Determining precisely the structure of such gels is not trivial, as shown by [16], and may play a crucial role on the confinement effects, which could explain the two different regimes observed on the velocity profiles. Indeed, enhancements of

the flows are observed for high-stirred and homogeneous Carbopol in microchannels as the opposite effect is observed for hand-stirred samples. A further step of this study would be to probe different confinements and to analyze some events —rearrangements— that we recorded during the flows. This would help to be more quantitative towards the link between the typical size of the microstructure and the cooperativity length ξ. To conclude, this work shows that Herschel-Bulkley flow curve has to be generalized to account for confined flows of polymer microgels, in order to take into account cooperative and non-local effects.

We thank Y. Forterre for providing us with the Carbopol, N. Louvet for helping us with the fabrication of the microchannels and A. Piednoir for the AFM measurements of the wall roughnesses. We deeply thank C. Cottin-Bizonne and C. Ybert for substantial help with the micro-PiV experimental device and H. Delanoë-Ayari for helping us with the tracking program. A. Colin, A.-L. Biance, E. Woillez and T. Divoux are thanked for enlightening discussions and constructive comments. We acknowledge support from the ANR, through the program "ANR Blanche" (Maniphyc).

Appendix A. Rheological flow curves of a YSF in a PP geometry versus a CP geometry

In this section we just recall how to take into account the stress inhomogeneity on the upper plate of a PP rheometer. This effect has already been understood and verified experimentally [25,26]. We chose to perform rheological measurements in a PP geometry for two reasons, first because slippage on smooth surface (such as the cone one) can dramatically change the flow curve at low shear rates, and thus lead to errors on the estimate of the HB coefficients. It is possible to counteract this problem in the PP geometry by gluing rough sand-paper on the planes to prevent slippage. The second reason is that we can study with pp geometry, the influence of the gap on the rheological curve and on the HB parameters.

On the other hand, a disadvantage of this geometry is that the shear rate is not homogeneous in the whole sample which leads to errors in the measured flow curve for non-Newtonian fluids. During the flow, the fluid is between two disks of radius R; the rheometer imposes a rotation speed Ω deforming at the maximum shear rate $\dot{\gamma}_{\max}$ and records the torque around the rotation axis M, which is related to the maximum shear stress $\sigma_{\max}$. Indeed, the torque corresponds to the sum of the shear stress $\sigma_{\theta z} = \sigma$ on the surface of the disk

$$M = \int_0^{2\pi} \int_0^R r \cdot \sigma(r) r \mathrm{d}r \, \mathrm{d}\theta. \qquad \text{(A.1)}$$

Defining the shear rate as the ratio of the velocity of the fluid at the upper plate divided by the height of fluid sheared between the two disks H, we have $\dot{\gamma}(r) = \frac{\Omega r}{H}$. Note that because of the geometry, the shear stress is not homogeneous on the surface of the upper disk, which is not the case in the cone-plate geometry. Indeed, in CP, $\dot{\gamma}$ is uniform in all the sample, and so σ, which leads to the proportionality of σ and M in eq. (A.1). If the fluid obeys an HB law, eq. (A.1) leads to

$$M = \frac{2\pi R^3}{3} \left\{ \sigma_Y + \frac{3K}{n+3} \dot{\gamma}_{\max}^n \right\}, \qquad \text{(A.2)}$$

which is interpreted by the rheometer as the torque supplied to shear a simple fluide $M = \frac{\pi R^3}{2} \sigma_{\mathrm{rec}}$. The recorded value of the shear stress is then

$$\sigma_{\mathrm{rec}} = \frac{4}{3} \left\{ \sigma_Y + \frac{3K}{n+3} \dot{\gamma}_{\max}^n \right\}, \qquad \text{(A.3)}$$

which is slightly different from the actual value $\sigma = \sigma_Y + K\dot{\gamma}_{\max}^n$. Figure 17 shows the difference between two experimental flow curves of the same sample obtained in CP and PP geometry before and after correction of the data. Note that the correct values of the HB coefficients are lower than the ones recorded directly with the PP geometry. Figure 17 also shows the collapse of the data of the CP-flow curve and the *corrected* PP-flow curve on a single master curve that really describes the flow of the fluid. The measurement uncertainty of the HB coefficient obtained in the PP geometry is about 1.3%.

To conclude, the PP geometry allows to get the HB coefficients of a YSF with a precision below 1.5% and to avoid problems of slippage. Note that the obtained coefficients are lower than the ones we would record without applying the correction (A.3), which could lead to some mistakes when we would compare the microscopic rheology to the macroscopic one.

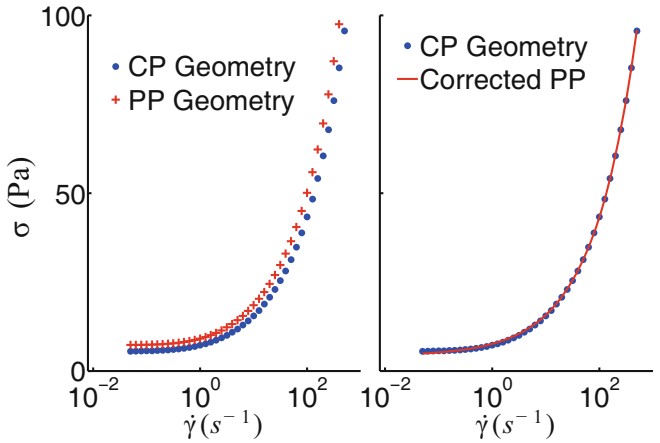

Fig. 17. Comparison between the flows curves of Carbopol 0.5% wt obtained with CP and PP geometries, before (left) and after (right) taking into account the correction due to the shear rate inhomogeneity with PP (see eq. (A.3)).

Appendix B. Study of the confined hand-stirred Carbopol

In this section we describe the experiments performed with the hand-stirred Carbopol samples. Because of the

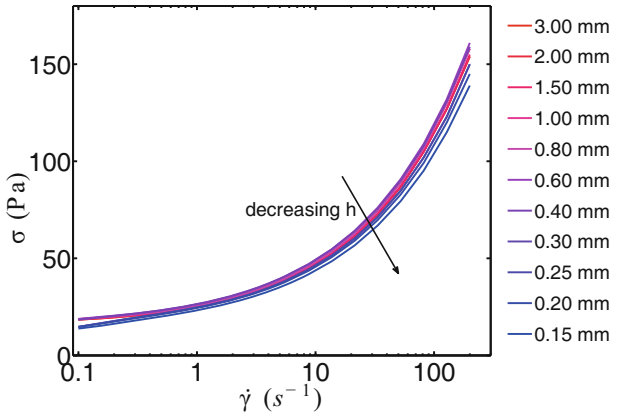

Fig. 18. Influence of the gap between the two planes on the flow curves of hand-stirred Carbopol 0.5% wt, swelled with NaOH, with 20 μm roughness plates. Each point is obtained by averaging over 30 s.

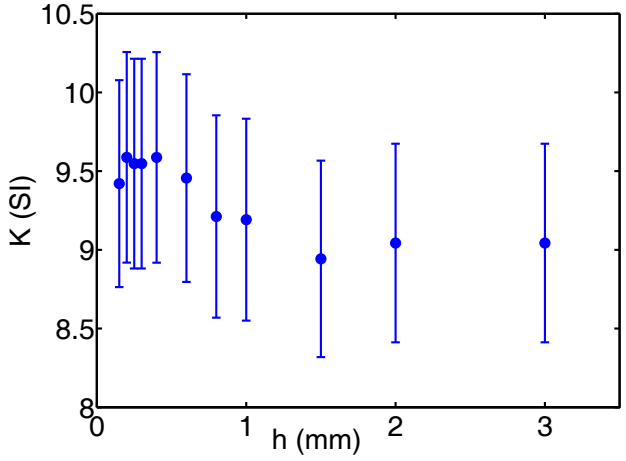

Fig. 19. Evolution of the HB consistency obtained by fitting the flow curves as a function of the gap values. The increase of K while the gap is decreased, is consistent with the flow reduction observed in the microchannel experiments (fig. 13) but the data dispersion does not allow to extract any typical length.

low stirring during their preparation, their microstructures are more heterogeneous than the high-stirred samples whose bigger polymer blobs are broken with the mixer. This leads to different behaviors of the gels under confinement, as shown in the following rheological and microscopical experiments. We follow the same procedure as for the other samples.

Influence of the confinement on the flow curves

Confinement effects on these samples can still be observed with a rheometer as shown in fig. 18. For these experiments, we measured the flow curves, for several gap values, of a hand-stirred Carbopol 0.5% wt in the PP geometry whose roughness is 20 μm.

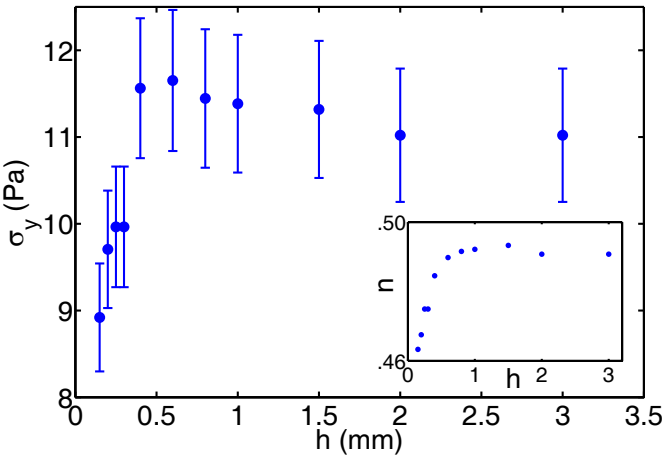

Fig. 20. Evolution of HB yield stress obtained by fitting the flow curves as a function of the gap values. The decrease of σ_y while the gap is reduced is due to slippage effect at low shear rates. Inset: corresponding HB exponent values.

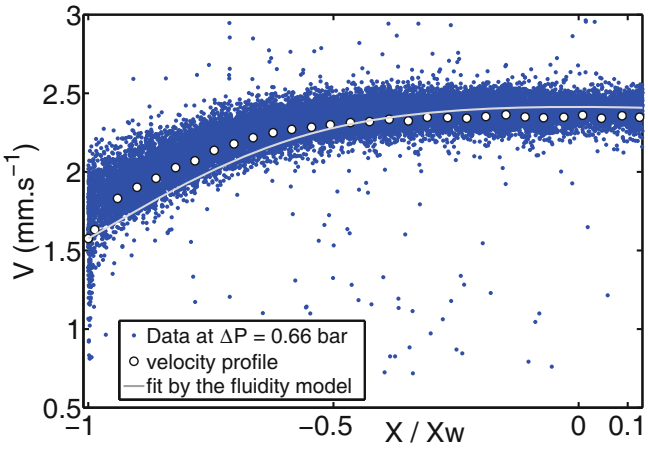

Fig. 21. Velocity profile of a hand-stirred Carbopol 0.5% wt with a pressure difference of 0.66 bar. Blue dots: data measured from the particle tracking step. White points: velocity profile after the binning process. Gray line: fit with the simple fluidity model.

Contrary to the experiments with high-stirred Carbopol, slippage effects at small shear rates are observed for gap values smaller than 400 μm. This indicates that the sample contains polymer blobs whose sizes are bigger than the plane roughness, *i.e.*, 20 μm. The existence of large microstructure is a consequence of the preparation and of the low stirring process. Moreover, fitting the flow curves with HB does not allow to find any typical length scale, as it was done in the case of high-stirred Carbopol (see sect. 3.2). Indeed, the consistency does not vary enough with the gap to get a typical length (fig. 19), while the obtained yield stress seems to decrease when the gap is reduced which is a direct consequence of the slippage (fig. 20). Nonetheless, the fact that the consistency slightly increases with confinement is consistent with the flow reductions observed in microchannels and shown in fig. 13.

The behavior of the samples under confinement makes the flow curves difficult to analyse quantitatively, but is a signature of a complex dynamic as shown with microscopic observations.

Microscopic velocity profiles and description

The velocity profiles of hand-stirred samples appear to be much more complicated to analyze than the ones obtained with highly stirred samples. Figure 21 presents a flow of the sample C1 (0.5% wt, hand stirred and swelled with NaOH). The data are much more noisy for these samples, especially close to the wall where the dispersion of the recorded velocities dramatically increases. This leads to a huge uncertainty for the estimation of the slip velocity which makes the analysis of the local rheology of hand-stirred samples more delicate. In particular, the velocity profile obtained after the binning process (white dots in fig. 21) presents a high variation of shear rate near the wall. This high shear rate near the wall makes the velocity profile impossible to analyse with the simple fluidity model, indeed the fluidity velocity profiles are very sensitive to the wall fluidity value. For these profiles, the wall fluidity is too high to allow the profile to adapt to the maximum velocity, and the two-free-parameters fit does not work well as shown in fig. 21 (gray curve). This feature is a direct consequence of the sample preparation and thus of their microstructure. The fact that the fluidity model does not fit well the data reflects the heterogeneity of the microstructure and thus the fact that ξ is not as well defined contrary to the case of high-stirred samples.

References

1. C.A. Angell, Science **267**, 1924 (1995).
2. P. Coussot, Soft Matter **3**, 528 (2007).
3. D. Bonn, M.M. Denn, Science **324**, 1401 (2009).
4. P.C.F. Møller, A. Fall, D. Bonn, EPL **87**, 38004 (2009).
5. B. Dollet, J. Rheol. **54**, 741 (2010).
6. R. Lespiat, S. Cohen-Addad, R. Höhler, Phys. Rev. Lett. **106**, 148302 (2011).
7. M. Le Merrer, S. Cohen-Addad, R. Höhler, Phys. Rev. Lett. **108**, 188301 (2012).
8. R. Besseling, L. Isa, P. Ballesta, G. Petekidis, M.E. Cates, W.C.K. Poon, Phys. Rev. Lett. **105**, 268301 (2010).
9. J. Goyon, A. Colin, G. Ovarlez, A. Ajdari, L. Bocquet, Nature **454**, 84 (2008).
10. J. Goyon, A. Colin, L. Bocquet, Soft Matter **6**, 2668 (2010).
11. P. Jop, V. Mansard, P. Chaudhuri, L. Bocquet, A. Colin, Phys. Rev. Lett. **108**, 148301 (2012).
12. K. Nichol, A. Zanin, R. Bastien, E. Wandersman, M. van Hecke, Phys. Rev. Lett. **104**, 078302 (2010).
13. K.A. Reddy, Y. Forterre, O. Pouliquen, Phys. Rev. Lett. **106**, 108301 (2011).
14. K. Kamrin, G. Koval, Phys. Rev. Lett. **108**, 178301 (2012).
15. M. Sbragaglia, R. Benzi, M. Bernaschi, S. Succi, Soft Matter **8**, 10773 (2012).
16. David Lee, Iris A. Gutowski, Arthur E. Bailey, Laurent Rubatat, John R. de Bruyn, Barbara J. Frisken, Phys. Rev. E **83**, 031401 (2011).
17. G. Benmouffok-Benbelkacem, F. Caton, C. Baravian, S. Skali-Lami, Rheol. Acta **49**, 305 (2010).
18. J.M. Piau, J. Non-Newtonian Fluid Mech. **144**, 1 (2007).
19. P. Coussot, L. Tocquer, C. Lanos, G. Ovarlez, J. Non-Newtonian Fluid Mech. **158**, 85 (2009).
20. T. Divoux, D. Tamarii, C. Barentin, S. Teitel, S. Manneville, Soft Matter **8**, 4151 (2012).
21. L. Bocquet, A. Colin, A. Ajdari, Phys. Rev. Lett. **103**, 036001 (2009).
22. G.P. Roberts, H.A. Barnes, Rheol. Acta **40**, 499 (2001).
23. L. Baudonnet, J.-L. Grossiord, F. Rodriguez, J. Dispersion Sci. Technol. **25**, 183 (2004).
24. J.-Y Kim, J.-Y. Song, E.-J. Lee, S.-K. Park, Colloid Polym. Sci. **281**, 614 (2003).
25. P. Schummer, R.H. Worthoff, Chem. Engen. Sci. **33**, 759 (1978).
26. M.S. Carvalho, M. Padmanabhan, C.W. Macosko, J. Rheol. **38**, 1925 (1994).
27. Y. Yan, Z. Zhang, D. Cheneler, J.R. Stokes, M.J. Adams, Rheol. Acta **49**, 255 (2010).
28. T. Divoux, D. Tamarii, C. Barentin, S. Manneville, Phys. Rev. Lett. **104**, 208301 (2010).
29. F.K. Oppong, L. Rubatat, A.E. Bailey, B.J. Frisken, J.R. de Bruyn, Phys. Rev. E **73**, 041405 (2006).
30. I.A. Gutowski, D. Lee, J.R. de Bruyn, B.J. Frisken, Rheol. Acta **51**, 441 (2012).
31. C. Métivier, Y. Rharbi, A. Magnin, A. Bou Abboud, Soft Matter **8**, 3365 (2012).
32. P. Guillot, P. Panizza, J.-B. Salmon, M. Joanicot, A. Colin, C.-H. Bruneau, T. Colin, Langmuir **22**, 6438 (2006).
33. S.P. Meeker, R.T. Bonnecaze, M. Cloitre, Phys. Rev. Lett. **92**, 198302 (2004).
34. S.P. Meeker, R.T. Bonnecaze, M. Cloitre, J. Rheol. **48**, 1295 (2004).